SECURITY CLASSIFICATION OF THIS PAGE (When Data Entered)

REPORT DOCUMENTATION PAGE

READ INSTRUCTIONS BEFORE COMPLETING FORM

1. REPORT NUMBER
NRL Report 7680

2. GOVT ACCESSION NO.

3. RECIPIENT'S CATALOG NUMBER

4. TITLE (and Subtitle)
CAPILLARITY-LIMITED STEADY-STATE DENDRITIC GROWTH, PART 2 — NUMERICAL RESULTS

5. TYPE OF REPORT & PERIOD COVERED
Final report on one phase of a continuing NRL Problem, October 1972 to October 1973.

6. PERFORMING ORG. REPORT NUMBER

7. AUTHOR(s)
Gerald E. Nash

8. CONTRACT OR GRANT NUMBER(s)

9. PERFORMING ORGANIZATION NAME AND ADDRESS
Naval Research Laboratory
Washington, D.C. 20375

10. PROGRAM ELEMENT, PROJECT, TASK AREA & WORK UNIT NUMBERS
NRL Problem M01-23
RR 022-01-46-5430

11. CONTROLLING OFFICE NAME AND ADDRESS
Department of the Navy
Office of Naval Research
Arlington, Virginia 22217

12. REPORT DATE
March 28, 1974

13. NUMBER OF PAGES
31

14. MONITORING AGENCY NAME & ADDRESS(if different from Controlling Office)

15. SECURITY CLASS. (of this report)
Unclassified

15a. DECLASSIFICATION/DOWNGRADING SCHEDULE

16. DISTRIBUTION STATEMENT (of this Report)
Approved for public release; distribution unlimited

17. DISTRIBUTION STATEMENT (of the abstract entered in Block 20, if different from Report)

18. SUPPLEMENTARY NOTES

19. KEY WORDS (Continue on reverse side if necessary and identify by block number)

Dendritic growth	Solidification
Diffusional transformations	Crystal structure
Capillarity	Microstructures
Supercooling	Crystal growth

20. ABSTRACT (Continue on reverse side if necessary and identify by block number)

The linearized equations describing nonisothermal, steady-state dendritic growth are solved numerically, and the relation between growth rate and supercooling is ascertained. For small supercoolings, the growth rate-supercooling relation is $V = 0.057\,(2\alpha_\ell \Delta S_f L/\gamma_{s\ell} c_\ell)[\Delta T/(L/c_\ell)]^{2.65}$, where V is the growth rate, ΔT is the supercooling, ΔS_f is the entropy of fusion per unit volume, L is the latent heat of fusion, $\gamma_{s\ell}$ is the solid/liquid interfacial free energy, and α_ℓ and c_ℓ are the thermal diffusivity and specific heat of the liquid respectively. The theoretically predicted growth

DD FORM 1 JAN 73 1473 EDITION OF 1 NOV 65 IS OBSOLETE
S/N 0102-014-6601

SECURITY CLASSIFICATION OF THIS PAGE (When Data Entered)

rates agree with those predicted by the "modified Ivantsov" analysis at high supercoolings and are higher than those predicted by the Bolling-Tiller-Temkin approach (by a factor of 2.3 at low supercoolings).

CONTENTS

INTRODUCTION 1

FINITE-DIFFERENCE SOLUTION OF THE LINEARIZED STEADY-STATE EQUATION 1

Finite-Difference Formulation 1
Calculation of the Curvature Change 7
Numerical Results 8

ESTIMATION OF λ_{max} 11

Computation of λ^* 11
Computation of λ^{**} 12

COMPARISON WITH PREVIOUS THEORETICAL RESULTS . 14

λ_{max} Predictions 14
Tip-Radius Predictions 15

COMPARISON WITH EXPERIMENTAL DATA 16

SUMMARY OF PART 2 19

REFERENCES 20

APPENDIX A — The Behavior of $C_1(r, s)$ and $C_2(r, s)$ as $s \to r$ and Numerical Computation Procedures 22

CAPILLARITY-LIMITED STEADY-STATE DENDRITIC GROWTH
PART 2 — NUMERICAL RESULTS

INTRODUCTION

In this report the theory developed in Part 1 (the companion report cited on the inside front cover) is implemented numerically. Specifically, techniques are developed for the solution of the linearized steady-state equation (Eq. (75) in Part 1) and for the estimation of λ_{max}, that is, the computation of λ^* and λ^{**} (the two subsections after Eq. (75) in Part 1). Numerical results are presented for small supercoolings ($0.01 \leqslant \Delta\Theta \leqslant 0.2$), and the estimated values of λ_{max} are compared to previous theoretical results [1-3] and to experiments [4-7]. A major finding is that the growth rates predicted by the theory are significantly higher than those predicted by the Bolling-Tiller [8] and Temkin [9] approach, which ignores the essential free-boundary nature of the dendrite problem.

FINITE-DIFFERENCE SOLUTION OF THE LINEARIZED STEADY-STATE EQUATION

Finite-Difference Formulation

An estimate of the shape change induced by the nonisothermality, $\delta\nu(y)$, may be obtained by solving Eq. (75) in Part 1 or equivalently by solving the equation

$$M_2'^{\omega_0}(0)\,\langle\nu^*\rangle = \frac{\nu^*(y)}{\xi^{1/2}(y)} - \int_0^\infty C_1(y,q)\,\nu^*(q)\,dq - \int_0^\infty C_2(y,q)$$

$$\times\left\{\left[\frac{1}{\xi^{1/2}(q)}\left(1+\frac{1}{2a_0}\right)+\frac{1}{a_0\xi^{3/2}(q)}\right]\nu^*(q) + \frac{q}{a_0\xi^{1/2}(q)}\,\nu^{*\prime}(q)\right\}dq$$

$$= \frac{1+\xi(y)}{a_0\xi^{3/2}(y)}, \qquad \xi(y) = 1 + (y/a_0)^2\,, \tag{1}$$

for ν^* and setting $\delta\nu = \lambda\nu^*$ ($0 \leqslant \lambda < \lambda_{max}$). Here $C_1(y,q)$ is given by Eq. (76a) in Part 1, namely,

$$C_1(y,q) = \frac{q}{\pi}\,e^{-[\omega_0(y)-\omega_0(q)]}\left\{\frac{d}{dn_q}\,G[y,z,q,\omega_0(q)]\Big|_{z=\omega_0(y)}\right.$$

$$\left. + \frac{1}{2a_0\xi^{1/2}(q)}\,G[y,\omega_0(y),q,\omega_0(q)]\right\}$$

Manuscript submitted October 25, 1973.

which, from Eqs. (39) and (40) in Part 1, can be written

$$C_1(y,q) = \frac{q}{\pi} e^{-[\omega_0(y)-\omega_0(q)]} \int_{-1}^{+1} e^{-(a+bt)^{1/2}} \left(\frac{\sin\theta_0(q)}{2q(a+bt)^{1/2}} - \left[\frac{1}{a+bt} + \frac{1}{(a+bt)^{3/2}} \right] \right.$$

$$\left. \times \{(q+yt)\sin\theta_0(q) - [\omega_0(y)-\omega_0(q)]\cos\theta_0(q)\} \right) \frac{1}{(1-t^2)^{1/2}}\, dt\,, \tag{2}$$

and $C_2(y,q)$ is given by Eq. (76b) in Part 1, namely,

$$C_2(y,q) = \frac{q}{\pi} e^{-[\omega_0(y)-\omega_0(q)]}\, G[y, \omega_0(y), q, \omega_0(q)]\,,$$

which, from Eq. (39) in Part 1, can be written

$$C_2(y,q) = \frac{q}{\pi} e^{-[\omega_0(y)-\omega_0(q)]} \int_{-1}^{+1} e^{-(a+bt)^{1/2}} [(a+bt)(1-t^2)]^{-1/2}\, dt\,, \tag{3}$$

where

$$a = q^2 + y^2 + [\omega_0(y) - \omega_0(q)]^2\,, \tag{4}$$

$$b = 2yq\,, \tag{5}$$

$$\omega_0(y) = -y^2/2a_0\,, \tag{6a}$$

$$\omega_0(q) = -q^2/2a_0\,, \tag{6b}$$

$$\sin\theta_0(q) = \frac{q}{a_0\xi^{1/2}(q)}\,, \tag{7a}$$

$$\cos\theta_0(q) = \frac{1}{\xi^{1/2}(q)}\,, \tag{7b}$$

and a_0 is a function of the supercooling $\Delta\Theta$ and can be found by solving Eq. (51) in Part 1.

The integrals occurring in Eqs. (2) and (3) cannot in general be evaluated in closed form. The behavior of these integrals, as well as a procedure for computing them numerically, is discussed in Appendix A. Sufficient to say here is that $C_2(y,q)$ has a logarithmic singularity when $q = y$.

Equation (1) is a linear integro-differential equation of the Fredholm type and may be solved numerically by finite-difference methods, provided that the infinite limits appearing in the integrals and the singularity associated with $C_2(y,q)$ are treated properly.

The infinite limits are readily dealt with by transforming the independent variable such that the interval $[0,\infty]$ is mapped onto the interval $[0,1]$. Thus, letting

$$w = \frac{y}{A + y}, \tag{8a}$$

$$u = \frac{q}{A + q}, \tag{8b}$$

where A is an arbitrary constant,* Eq. (1) becomes

$$\frac{\nu^*(w)}{\xi^{1/2}(w)} - \int_0^1 C_1(w,u)\,\frac{A}{(1-u)^2}\,\nu^*(u)\,du$$

$$-\int_0^1 C_2(w,u)\,\frac{A}{(1-u)^2}\left\{\left[\frac{1}{\xi^{1/2}(u)}\left(1 + \frac{1}{2a_0}\right)\right.\right.$$

$$\left.\left. + \frac{1}{a_0\xi^{3/2}(u)}\right]\nu^*(u) + \frac{q(u)(1-u)^2}{a_0\xi^{1/2}(u)A}\,\nu^{*\prime}(u)\right\}du = \frac{1 + \xi(w)}{a_0\xi^{3/2}(w)}, \tag{9}$$

where

$$y(w) = \frac{Aw}{1 - w}, \tag{10a}$$

$$q(u) = \frac{Au}{1 - u}, \tag{10b}$$

$$\xi(w) = 1 + [y(w)/a_0]^2, \tag{10c}$$

$$\xi(u) = 1 + [q(u)/a_0]^2, \tag{10d}$$

$$C_1(w,u) = C_1[y(w), q(u)], \tag{10e}$$

$$C_2(w,u) = C_2[y(w), q(u)]. \tag{10f}$$

(Though the transformation defined by Eq. (8) does eliminate the infinite integrals in Eq. (1), it does so only at the price of introducing an additional singularity into the problem, namely, the factor $A/(1-u)^2$, which appears in the integrands in Eq. (9). However, since it can be shown that

$$\lim_{u\to 1} C_j(w,u) \quad (j = 1, 2)$$

*The selection of A is more or less dictated by experience. The values of A used in the numerical calculations will be tabulated later.

approaches zero faster than $(1-u)^2$ and that $\nu^*|_{q=\infty} = 0$, the additional singularity introduced by the transformation does not complicate the numerical solution.)

The logarithmic singularity in $C_2(w,u)$ can be treated by subtracting the singularity, a technique commonly used in evaluating improper integrals [10]. Thus, adding and subtracting the quantity

$$I = \int_0^1 C_2(w,u)\,\frac{A}{(1-u)^2}\left\{\left[\frac{1}{\xi^{1/2}(w)}\left(1+\frac{1}{2a_0}\right)+\frac{1}{a_0\xi^{3/2}(w)}\right]\nu^*(w)\right.$$

$$\left.+\frac{q(w)(1-w)^2}{a_0\xi^{1/2}(w)A}\,\nu^{*\prime}(w)\right\}du \tag{11}$$

to Eq. (9) and noting (with the aid of Eq. (48) in Part 1 with $\lambda = 0$, which is the isothermal solution) that

$$I = \left(\left[\frac{1}{\xi^{1/2}(w)}\left(1+\frac{1}{2a_0}\right)+\frac{1}{a_0\xi^{3/2}(w)}\right]\nu^*(w)+\frac{q(w)(1-w)^2}{a_0\xi^{1/2}(w)A}\,\nu^{*\prime}(w)\right)\int_0^\infty C_2(y,q)\,dq$$

$$= \left(\left[\frac{1}{\xi^{1/2}(w)}\left(1+\frac{1}{2a_0}\right)+\frac{1}{a_0\xi^{3/2}(w)}\right]\nu^*(w)+\frac{q(w)(1-w)^2}{a_0\xi^{1/2}(w)A}\,\nu^{*\prime}(w)\right)\Delta\Theta\,, \tag{12}$$

Eq. (9) becomes

$$M_2^{\prime\omega_0}(0)\,\langle\nu^*\rangle = \frac{\nu^*(w)}{\xi^{1/2}(w)} - \int_0^1 \bar{C}_1(w,u)\nu^*(u)\,du - \int_0^1 \bar{C}_2(w,u)\,[\phi_1(u)\,\nu^*(u)$$

$$+\phi_2(u)\nu^{*\prime}(u) - \phi_1(w)\nu^*(w) - \phi_2(w)\nu^{*\prime}(w)]\,du$$

$$-[\phi_1(w)\nu^*(w) + \phi_2(w)\nu^{*\prime}(w)]\,\Delta\Theta$$

$$= \frac{1+\xi(w)}{a_0\xi^{3/2}(w)}\,, \tag{13}$$

where

$$\bar{C}_j(w,u) = C_j(w,u)\,\frac{A}{(1-u)^2}\,, \qquad j = 1,\,2, \tag{14a}$$

$$\phi_1(z) = \frac{1}{\xi^{1/2}(z)}\left(1+\frac{1}{2a_0}\right)+\frac{1}{a_0\xi^{3/2}(z)}\,, \tag{14b}$$

$$\phi_2(z) = \frac{q(z)(1-z)^2}{a_0\xi^{1/2}(z)A}\,. \tag{14c}$$

If the function $\phi_1(z)\nu^*(z) + \phi_2(z)\nu^{*\prime}(z)$ satisfies a Hölder condition, namely,

$$|\phi_1(u)\nu^*(u) + \phi_2(u)\nu^{*\prime}(u) - \phi_1(w)\nu^*(w) - \phi_2(w)\nu^{*\prime}(w)| < C|u - w|^\gamma , \qquad (15)$$

where C and γ are constants with $0 < \gamma \leqslant 1$, then the integrand involving $\bar{C}_2(w,u)$ is zero when $u = w$ and $\bar{C}_2(w,w)$ can be defined arbitrarily. In subsequent work we shall assume that $\nu^*(w)$ is such that Eq. (15) is always satisfied.

To solve Eq. (13) numerically, the interval $[0,1]$ is partitioned into N subintervals $[w_i, w_{i+1}]$ $(i = 0, 1, 2, \ldots, N-1)$ with $w_i = i/N$ $(i = 0, 1, 2, \ldots, N)$, and it is assumed that Eq. (13) is satisfied at the points w_i $(i = 0, 1, 2, \ldots, N-1)$. Thus

$$\frac{\nu^*(w_i)}{\xi^{1/2}(w_i)} - \int_0^1 \bar{C}_1(w_i,u)\nu^*(u)\,du$$

$$- \int_0^1 \bar{C}_2(w_i,u)[\phi_1(u)\nu^*(u)$$

$$+\phi_2(u)\nu^{*\prime}(u) - \phi_1(w_i)\nu^*(w_i) - \phi_2(w_i)\nu^{*\prime}(w_i)]\,du$$

$$+[\phi_1(w_i)\nu^*(w_i) + \phi_2(w_i)\nu^{*\prime}(w_i)]\,\Delta\Theta = \frac{1 + \xi(w_i)}{a_0\xi^{3/2}(w_i)}, \qquad i = 0, 1, \ldots, N-1 . \qquad (16)$$

By approximating the integrals and derivatives above by trapezoidal quadrature and central differences respectively and assuming that the solutions approach zero as $y \to \infty$ $(\nu^*(w_N) = \nu^*(1) = 0)$ and that the solutions are symmetric in w $(\nu^{*\prime}(0) = 0)$, the following system of simultaneous equations for $\nu^*(w_i)$ $(i = 0, 1, \ldots, N)$ is obtained:

$$\frac{\nu_0^*}{\xi_0^{1/2}} - \frac{h}{2}\bar{C}_{100}\nu_0^* - h\sum_{j=1}^{N-1}\left\{\bar{C}_{10j}\nu_j^*\right.$$

$$+\bar{C}_{20j}\left[\phi_{1j}\nu_j^* + \phi_{2j}\left(\frac{\nu_{j+1}^* - \nu_{j-1}^*}{2h}\right)\right.$$

$$\left.\left.-\phi_{10}\nu_0^*\right]\right\} - \phi_{10}\nu_0^*\Delta\Theta = \frac{1 + \xi_0}{a_0\xi_0^{3/2}}, \qquad (17a)$$

$$\frac{\nu_i^*}{\xi_i^{1/2}} - \frac{h}{2}\left\{\bar{C}_{1i0}\nu_0^* + \bar{C}_{2i0}\left[\phi_{10}\nu_0^* - \phi_{1i}\nu_i^* - \phi_{2i}\left(\frac{\nu_{i+1}^* - \nu_{i-1}^*}{2h}\right)\right]\right\} - h\sum_{j=1}^{N-1}\left\{\bar{C}_{1ij}\nu_j^* + \bar{C}_{2ij}\left[\phi_{ij}\nu_j^* + \phi_{2j}\left(\frac{\nu_{j+1}^* - \nu_{j-1}^*}{2h}\right) - \phi_{1i}\nu_i^* - \phi_{2i}\left(\frac{\nu_{i+1}^* - \nu_{i-1}^*}{2h}\right)\right]\right\} - \left[\phi_{1i}\nu_i^* + \phi_{2i}\left(\frac{\nu_{i+1}^* - \nu_{i-1}^*}{2h}\right)\right]\Delta\Theta = \frac{1 + \xi_i}{a_0\xi_i^{3/2}}, \quad i = 1, 2, \ldots, N - 1 \tag{17b}$$

$$\nu_N = 0, \tag{17c}$$

where

$$h = 1/N, \tag{18a}$$

$$\nu_i^* = \nu^*(i/N), \tag{18b}$$

$$\xi_i = \xi(i/N), \tag{18c}$$

$$\phi_{ki} = \phi_k(i/N)(k = 1, 2), \tag{18d}$$

$$\bar{C}_{kij} = \bar{C}_k(i/N, j/N)(k = 1, 2), \tag{18e}$$

and $\bar{C}_{2ii}$ is defined arbitrarily as zero. Equations (17), which can also be written in matrix notation as

$$\underset{\sim}{L}_2\underset{\sim}{\nu}^* = \underset{\sim}{C}, \tag{19}$$

where $\underset{\sim}{L}_2$ is an $N + 1$ by $N + 1$ matrix,

$$\underset{\sim}{\nu}^* = \begin{pmatrix} \nu_0^* \\ \nu_1^* \\ \cdots \\ \nu_N^* \end{pmatrix}, \tag{20a}$$

$$\underset{\sim}{C} = \begin{pmatrix} (1+\xi_0)/a_0\xi_0^{3/2} \\ (1+\xi_1)/a_0\xi_1^{3/2} \\ \cdots \\ (1+\xi_N)/a_0\xi_N^{3/2} \end{pmatrix}, \tag{20b}$$

can be solved by standard methods. Selected results will be presented following the next subsection.

Calculation of the Curvature Change

In addition to $\delta\nu$ the curvature change $\delta\kappa(w)$ induced by the nonisothermality is also of interest, particularly in the computation of λ^* to follow later. The curvature change $\delta\kappa(w)$ and its finite-difference representation can be calculated as follows. From Part 1 the curvature change $\delta\kappa(w)$ associated with $\delta\nu(w)$ is given by

$$\delta\kappa(w) = M_1'^{\omega_0}(0)\,\langle\delta\nu\rangle = \lambda M_1'^{\omega_0}(0)\,\langle\nu^*\rangle\,, \tag{21}$$

where ν^* is a solution to Eq. (16) and

$$M_1'^{\omega_0}(0)\,\langle\nu^*\rangle = \frac{1}{\xi(w)}\left\{\frac{d^2}{dy^2}\,\nu^*[y(w)] + \frac{1}{y(w)\xi(w)}\,\frac{d}{dy}\,\nu^*[y(w)] + \frac{1}{a_0^{\,2}}\left[1+\frac{1}{\xi^2(w)}\right]\nu^*(w)\right\}, \qquad w \neq 0\,. \tag{22}$$

But from Eq. (8)

$$\frac{d}{dy}\,\nu^*[y(w)] = \frac{(1-w)^2}{A}\,\nu^{*\prime}(w) \tag{23a}$$

and

$$\frac{d^2}{dy^2}\,\nu^*[y(w)] = \frac{(1-w)^4}{A^2}\,\nu^{*\prime\prime}(w) - \frac{2(1-w)^3}{A^2}\,\nu^{*\prime}(w)\,. \tag{23b}$$

Therefore

$$M_1'^{\omega_0}(0)\,\langle\nu^*\rangle = \frac{1}{\xi(w)}\left\{\frac{(1-w)^4}{A^2}\,\nu^{*\prime\prime}(w) + \frac{(1-w)^2}{A}\left[\frac{1}{y(w)\xi(w)} - \frac{2(1-w)}{A}\right]\nu^{*\prime}(w) + \frac{1}{a_0^{\,2}}\left[1+\frac{1}{\xi^2(w)}\right]\nu^*(w)\right\}, \qquad w \neq 0\,. \tag{24a}$$

At the tip ($w = 0$), Eq. (24a) becomes (by Eq. (10) and L'Hôpital's rule)

$$M_1'^{\omega_0}(0)\,\langle \nu^* \rangle = \nu^{*\prime\prime}(0) + \frac{2}{a_0}\,\nu^*(0) + \lim_{w \to 0} \frac{\nu^{*\prime}(w)}{y(w)}$$

$$= 2\left[\frac{1}{A^2}\,\nu^{*\prime\prime}(0) + \frac{1}{a_0^2}\,\nu^*(0)\right]. \tag{24b}$$

The finite difference forms of Eqs. (24) are readily obtained by employing central difference approximations for $\nu^{*\prime}(w)$ and $\nu^{*\prime\prime}(w)$. Thus

$$\frac{\delta\kappa(w_i)}{\lambda} = M_1'^{\omega_0}(0)\,\langle \nu^* \rangle$$

$$= \frac{1}{\xi_i}\left\{\frac{(1-w_i)^4}{A^2}\left(\frac{\nu_{i+1}^* - 2\nu_i^* + \nu_{i-1}^*}{h^2}\right) + \frac{(1-w_i)^2}{A}\left[\frac{1}{y_i\xi_i}\right.\right.$$

$$\left.\left. - \frac{2(1-w_i)}{A}\right]\left(\frac{\nu_{i+1}^* - \nu_{i-1}^*}{2h}\right) + \frac{1}{a_0^2}\left(1 + \frac{1}{\xi_i^2}\right)\nu_i^*\right\}, \qquad y_i = y(i/N)\,, \tag{25a}$$

and

$$\frac{\delta\kappa(0)}{\lambda} = M_1'^{\omega_0}(0)\,\langle \nu^* \rangle\big|_{w=0}$$

$$= \frac{4}{(Ah)^2}\,(\nu_1^* - \nu_0^*) + \frac{2}{a_0^2}\,\nu_0^*\,, \tag{25b}$$

where the symmetry condition $\nu^{*\prime}(0)$ was invoked in deriving Eq. (25b).

Numerical Results

Equation (19) was solved numerically for the range of supercoolings $0.01 \leqslant \Delta\Theta \leqslant 0.2$. The values of A and a_0 used in the numerical solutions are listed in Table 1. Representative solutions to Eq. (19) plotted as a function of y, are shown in Figs. 1 and 2 for $\Delta\Theta = 0.03$ and 0.07 respectively. The convergence with respect to N is good for both supercoolings. These results are typical of the behavior of the numerical solutions over the full range of supercoolings.*

*Additional checks on the reliability of the finite-difference procedure have been carried out for the two-dimensional version of this problem (platelet growth) by solving the linearized equations both by finite differences and Galerkin's method (a discussion of this method is given Mikhlin [11]). The solutions obtained by both methods agreed to within a few percent.

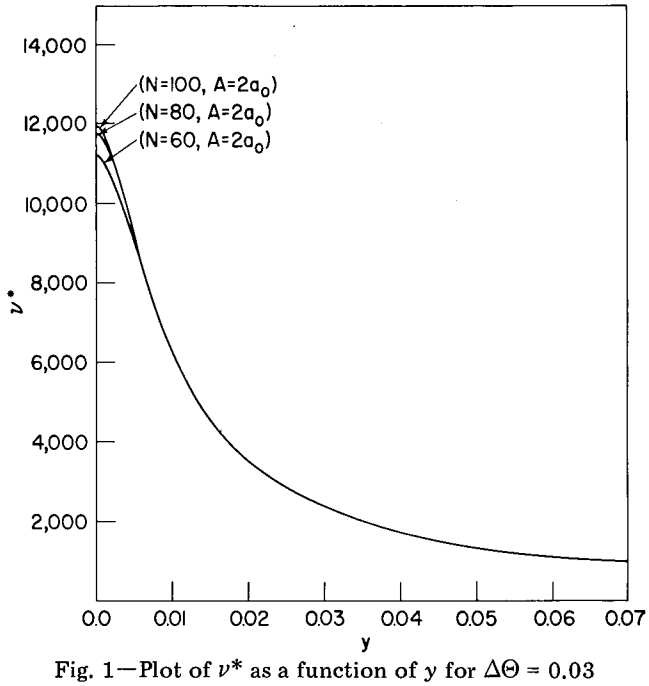

Fig. 1—Plot of ν^* as a function of y for $\Delta\Theta = 0.03$

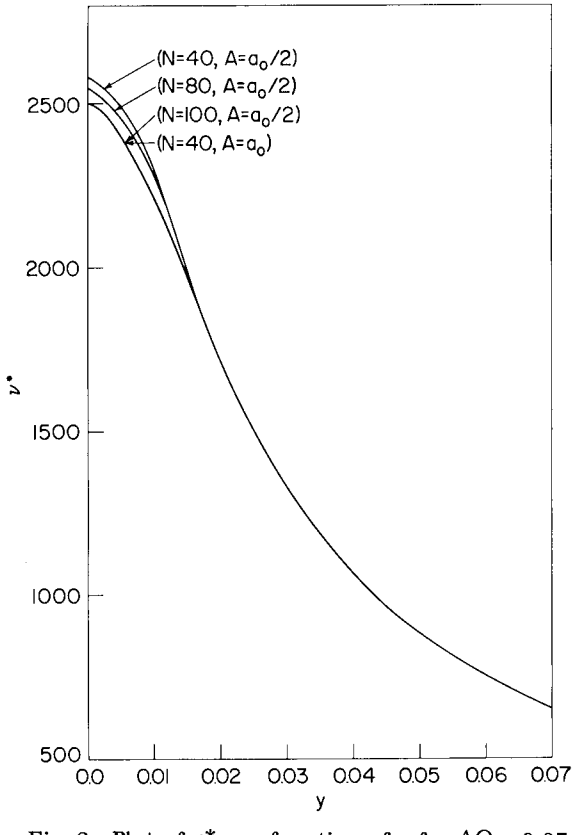

Fig. 2—Plot of ν^* as a function of y for $\Delta\Theta = 0.07$

Table 1
Values Used in Numerically Solving Eq. (19)

$\Delta\Theta$	a_0	A
0.01	1.73×10^{-3}	$4a_0$
0.03	6.72×10^{-3}	$2a_0$
0.05	0.0131	a_0
0.07	0.0206	a_0, $a/2$
0.1	0.0341	$a_0/2$
0.2	0.0988	$a_0/6$

The curvature changes associated with each of the preceding solutions were also calculated, with the aid of Eqs. (25). The quantity $-\delta\kappa(w)/\lambda$, also plotted as a function of y, is shown in Figs. 3 and 4 for $\Delta\Theta = 0.03$ and 0.07. From these results it is evident that the effect of the nonisothermal interface conditions is to sharpen the interface in the neighborhood of the tip and flatten it elsewhere.

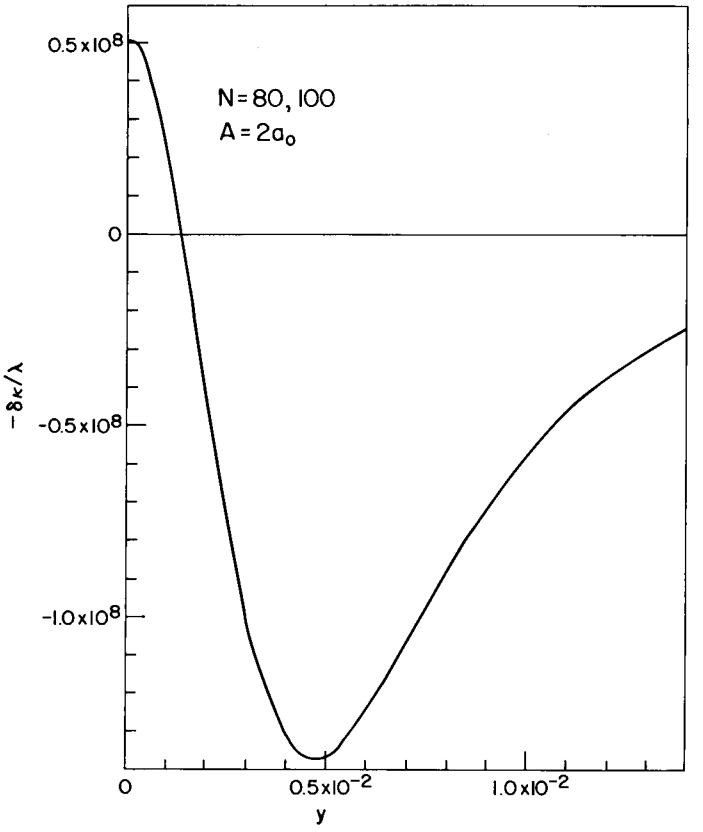

Fig. 3—Plot of $\delta\kappa/\lambda$ as a function of y for $\Delta\Theta = 0.03$

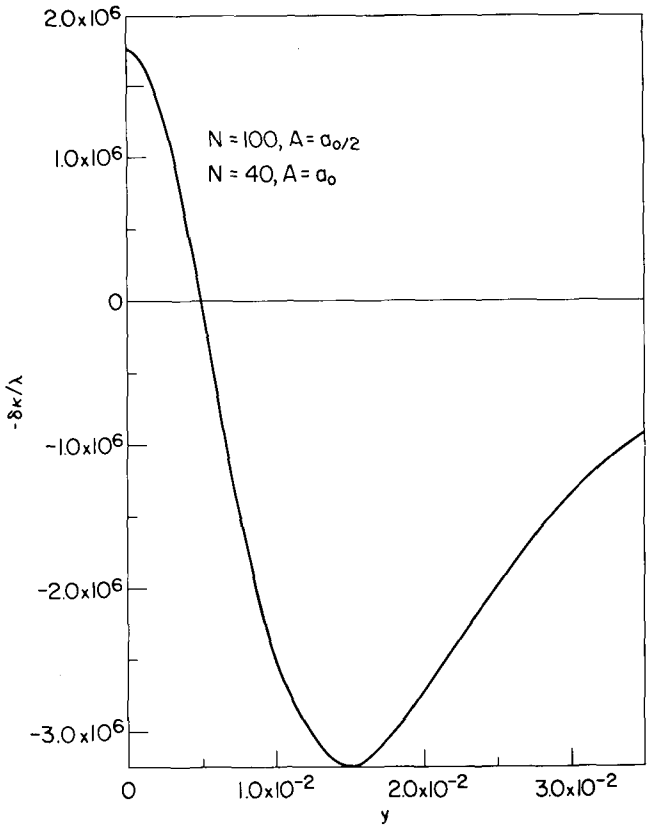

Fig. 4—Plot of $\delta\kappa/\lambda$ as a function of y for $\Delta\Theta = 0.07$

ESTIMATION OF λ_{max}

Computation of λ^*

It was shown in the subsection "λ_{max} Estimate" in Part 1 that a rigorous upper bound λ^*, on λ_{max}, is given by

$$\lambda^* = \frac{-2}{M_1'^{\omega_0}(0)\,\langle \nu^* \rangle|_{w=0} a_0} \tag{26}$$

or from Eq. (24b)

$$\lambda^* = \frac{-1}{\dfrac{a_0}{A^2}\,\nu^{*\prime\prime}(0) + \dfrac{1}{a_0}\,\nu^*(0)}, \tag{27}$$

where $\nu^* = \nu^*(w)$ is a solution to Eq. (16). Calculated values of λ^* are listed in Table 2 along with the quantity $-\lambda^*\kappa_0(0) = 2\lambda^*/a_0$, which is depicted graphically in Fig. 6 of Part 1

Table 2
Calculated Values of λ^* and $2\lambda^*/a_0$

$\Delta\Theta$	λ^*	$2\lambda^*/a_0$	$(2\lambda^*/a_0)/\Delta\Theta$
0.01	3.18×10^{-7}	3.68×10^{-4}	0.0368
0.03	5.94×10^{-6}	1.77×10^{-3}	0.0589
0.05	2.18×10^{-5}	3.33×10^{-3}	0.0665
0.07	5.47×10^{-5}	5.31×10^{-3}	0.0758
0.1	1.47×10^{-4}	8.62×10^{-3}	0.0862
0.2	1.09×10^{-3}	0.0218	0.109

It is apparent from Fig. 6 in Part 1 that the magnitude of the quantity $2\lambda^*/a_0$ gives at least a qualitative indication of how well λ^* approximates λ_{max}; that is, if $(2\lambda^*/a_0)/\Delta\Theta << 1$, then λ^* should be close to λ_{max}. Table 2 shows that $(2\lambda^*/a_0)/\Delta\Theta$ increases monotonically with $\Delta\Theta$ and ranges from 0.0368 for $\Delta\Theta = 0.01$ to 0.109 for $\Delta\Theta = 0.2$, thus indicating that the estimates provided by λ^* improve as the supercooling decreases. Moreover the values of $(2\lambda^*/a_0)/\Delta\Theta$ listed are relatively small compared with unity, thereby lending some credibility to the validity of the λ^* estimate.

Computation of λ^{**}

In the subsection "A Second λ_{max} Estimate" in Part 1, it was shown that an estimate λ^{**}, of λ_{max} could be found by finding the value of λ such that the equation

$$\lambda M_1'^{\omega_0}(0)\langle\delta\nu\rangle + M_2'^{\omega_0}(0)\langle\delta\nu\rangle = \lambda\left[\frac{1+\xi(y)}{a_0\xi^{3/2}(y)}\right] \tag{28}$$

fails to possess a solution. Here $M_k'^{\omega_0}(0)$ $(k = 1, 2)$ are defined implicitly in Eqs. (24) and (13) respectively.

To calculate λ^{**} numerically, the integrals and derivatives appearing in $M_k'^{\omega_0}(0)$ $(k = 1, 2)$ are again approximated by trapezoidal quadrature and central differences respectively, as was done in obtaining Eqs. (17). Then by assuming that Eq. (28) is identically satisfied at the points $w_i = i/N$ $(i = 0, 1, 2, \ldots, N-1)$ and employing the boundary conditions $[\delta\nu(0)]' = \delta\nu(1) = 0$, the following system of equations is obtained for $\delta\nu(w_i)$ $(i = 0, 1, 2, \ldots, N)$:

$$(\lambda \underset{\sim}{L}_1 + \underset{\sim}{L}_2)\delta\underset{\sim}{\nu} = \underset{\sim}{C}, \tag{29}$$

where $\delta\underset{\sim}{\nu}$ and $\underset{\sim}{C}$ are defined as in Eqs. (20), $\underset{\sim}{L}_2$ is the same matrix which appears in Eq. (19), $\underset{\sim}{L}_1$ is an $N + 1$ by $N + 1$ tridiagonal matrix with components

$$L_{100} = \frac{2}{a_0^2} - \frac{4}{(Ah)^2}, \tag{30a}$$

$$L_{102} = \frac{4}{(\mathrm{Ah})^2}, \tag{30b}$$

$$L_{10j} = 0, \quad j = 3, 4, \ldots, N, \tag{30c}$$

$$L_{1ij} = \left[\frac{(1-w_j)^4}{\xi_j(Ah)^2} - \frac{(1-w_j)^2}{\xi_j Ah}\left(\frac{1}{2y_j\xi_j} - \frac{1-w_j}{A}\right)\right]\delta_{i-1j}$$

$$+\left[\frac{1}{\xi_j a_0^2}\left(1 + \frac{1}{\xi_j^2}\right) - \frac{2(1-w_j)^2}{\xi_j(Ah)^2}\right]\delta_{ij}$$

$$+\left[\frac{(1-w_j)^4}{\xi_j(Ah)^2} + \frac{(1-w_j)^2}{\xi_j Ah}\left(\frac{1}{2y_j\xi_j} - \frac{1-w_j}{A}\right)\right]\delta_{i+1j}, \qquad \begin{array}{l} i = 1, 2, \ldots, N-1, \\ j = 0, 1, \ldots, N, \end{array} \tag{30d}$$

$$L_{1Nj} = 0, \quad j = 0, 1, \ldots, N, \tag{30e}$$

and δ_{ij} denotes the Kronecker delta. Since a unique solution to Eq. (29) does not exist when

$$\det(\lambda \underset{\sim}{L}_1 + \underset{\sim}{L}_2) = 0, \tag{31}$$

the smallest value of λ satisfying condition (31) constitutes an approximation to λ^{**}.

Finding the smallest value of λ which satisfies condition (31) is equivalent to finding smallest eigenvalue of the matrix $-\underset{\sim}{L}_1^{-1}\underset{\sim}{L}_2$, which is a standard problem in numerical analysis. Values of λ^{**} have been computed for $0.01 \leqslant \Delta\Theta \leqslant 0.2$ by the $Q - R$ algorithm [12] and are listed in Table 3, together with the corresponding values of λ^*.†

Table 3
Calculated Values of λ^{**} and Values of λ^*
From Table 2

$\Delta\Theta$	λ^{**}	λ^*
0.01	3.62×10^{-7}	3.18×10^{-7}
0.03	6.82×10^{-6}	5.94×10^{-6}
0.05	2.5×10^{-5}	2.18×10^{-5}
0.07	6.23×10^{-5}	5.47×10^{-5}
0.1	1.71×10^{-4}	1.47×10^{-4}
0.2	1.25×10^{-3}	1.08×10^{-3}

† Pursuant to the arguments presented in Part 1, Eq. (28) is expected to have no solutions when $\lambda > \lambda^{**}$. In other words the operator $-[M_1'^{\omega 0}(0)]^{-1} M_2'^{\omega 0}(0)$ is expected to have a continuous spectrum. However, since the matrix approximation to $-[M_1'^{\omega 0}(0)]^{-1} M_2'^{\omega 0}(0)$, namely, $-\underset{\sim}{L}_1^{-1}\underset{\sim}{L}_2$, can have only a discrete spectrum, an interesting question arises: What do the solutions to Eq. (29) look like when $\lambda > \lambda^{**}$? To resolve this question, a number of calculations were performed. In all cases the solutions were observed to be highly oscillatory, bearing no relation to the smooth solutions found for $\lambda < \lambda^{**}$.

As can be seen from the table, λ^* and λ^{**} are relatively close, with λ^{**} consistently greater than λ^* by a factor of approximately 1.15. This indicates that λ^{**} is also an upper bound on λ_{max}. Since λ^* is less than λ^{**}, λ^* will be taken as the estimate for λ_{max} when comparing the theory to previous theoretical results and experimental data.

COMPARISON WITH PREVIOUS THEORETICAL RESULTS

λ_{max} Predictions

The previous theoretical approaches to the steady-state dendritic growth problem can be grouped into two categories: the "modified Ivantsov" approach, developed by Sekerka et al. [1] and Glicksman and Schaefer [2], and the Bolling-Tiller [8] and Temkin [9] approach, which was later refined by Trivedi [13]. In this subsection the nondimensional relations between growth rate and supercooling predicted by both theories are compared to the relation between λ^* and $\Delta\Theta$ obtained from Eq. (27).

The relations between growth rate and supercooling obtained from each of the three approaches are shown in Fig. 5. For small supercoolings ($\Delta\Theta \leqslant 0.1$) each theory predicts a relation between growth rate and supercooling in the form of a power law:

$$\lambda_{max} = 0.057\,(\Delta\Theta)^{2.65} \quad \text{(present results)}\,, \tag{32a}$$

$$\lambda_{max} = 0.025\,(\Delta\Theta)^{2.65} \quad \text{(Trivedi [3])}\,, \tag{32b}$$

$$\lambda_{max} = 0.041\,(\Delta\Theta)^{2.21} \quad \text{("modified Ivantsov" [1,2])}\,. \tag{32c}$$

In general the "modified Ivantsov" approach predicts the highest growth rates, Trivedi's analysis predicts the lowest growth rates, and the present approach using Eq. (27) predicts growth rates in between. The $\lambda^* - \Delta\Theta$ curve obtained from Eq. (27) approaches the "modified Ivantsov" curve as the supercooling increases; an extrapolation together with λ^* estimates for $\Delta\Theta > 0.2$ (not presented here) suggests that the two curves should coalesce at $\Delta\Theta \approx 0.3 - 0.4$. Moreover the $\lambda^* - \Delta\Theta$ curve, obtained from Eq. (27) is almost exactly parallel to the curve based on Trivedi's analysis for $\Delta\Theta \leqslant 0.1$, though the growth rates predicted by the present analysis are higher than those predicted by Trivedi's analysis by a factor of 2.3.

The coalescence of the λ^* values with the "modified Ivantsov" predictions is particularly encouraging, because it can be plausibly argued on physical grounds that the "modified Ivantsov" predictions should be appropriate at high supercoolings. Moreover Glicksman and Schaefer [2] successfully used the "modified Ivantsov" analysis to fit their experimental data on white phosphorus for $0.2 < \Delta\Theta < 1.8$, with the best fit obtained at the higher supercoolings. Similar attempts to fit these data with the refinements of the Bolling-Tiller and Temkin approach were largely unsuccessful [14].

In view of the agreement of the λ^* values with the "modified Ivantsov" predictions for $\Delta\Theta > 0.3 - 0.4$ and the appropriateness of the "modified Ivantsov" analysis for this range of supercoolings, it is reasonable to expect the λ^* values to provide good estimates of λ_{max} for $\Delta\Theta \approx 0.2$. Moreover, as was indicated by Table 2, the estimates of λ_{max} provided by λ^* should improve as the supercooling decreases. It therefore follows that

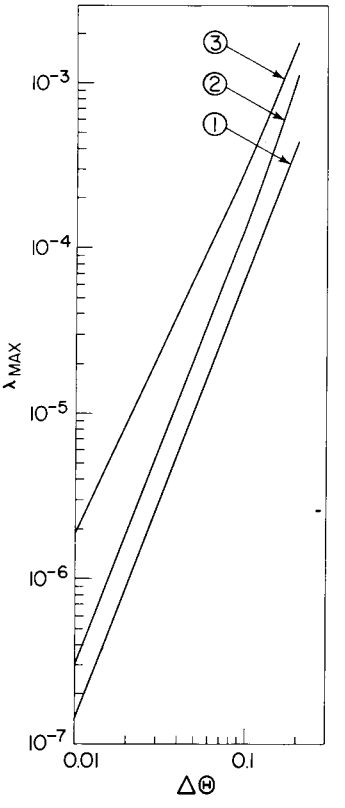

Fig. 5—Plot of λ_{max} as a function of $\Delta\Theta$ for (1) the Trivedi analysis [3], (2) the present analysis using Eq. (27), and (3) the modified Ivantsov analysis [1,2]

the entire $\lambda^* - \Delta\Theta$ curve shown in Fig. 5 gives a good approximation to the $\lambda_{max} - \Delta\Theta$ curve. Thus it appears that the values of λ_{max} predicted by Trivedi's analysis are indeed low.

Tip-Radius Predictions

In addition to λ_{max} the nondimensional dendrite tip radius $a(0) \equiv -2/\kappa(0)$ at $\lambda = \lambda_{max}$ is also of interest and can be estimated as follows. By definition

$$\kappa(0) = \kappa_0(0) + \delta\kappa(0) . \tag{33}$$

But $\kappa_0(0) = -2/a_0$ and

$$\delta\kappa(0) \approx \lambda^* M_1'^{\omega_0}(0) \langle \nu^* \rangle|_{w=0} = -2/a_0 , \quad \lambda = \lambda_{max} , \tag{34}$$

by Eqs. (21) and (26). Therefore

$$\kappa(0) \approx -4/a_0 , \quad \lambda = \lambda_{max} ; \tag{35}$$

hence

$$a(0) \approx a_0/2 . \tag{36}$$

That is, the tip radius at $\lambda = \lambda_{max}$ is approximately half the isothermal tip radius.*

The nondimensional tip radii predicted by Eq. (36) are shown in Fig. 6 as a function of $\Delta\Theta$ along with the predictions of the "modified Ivantsov" analysis. The predictions of both theories agree to within a few percent for $\Delta\Theta < 0.6$. For $\Delta\Theta > 0.6$ the predictions of the two theories diverge, with the tip radii predicted by the "modified Ivantsov" analysis significantly less than those predicted by Eq. (36). Because the "modified Ivantsov" analysis is valid for this range of supercoolings, it is concluded that the estimates of a_0 given by Eq. (36) (and most likely the estimates of λ_{max} provided by λ^*) represent poor approximations for $\Delta\Theta > 0.6$. Finally, little significance should be attached to the agreement of the tip radii predictions for $\Delta\Theta < 0.3 - 0.4$, since the growth rates predicted by the "modified Ivantsov" analysis are incorrect for these supercoolings.

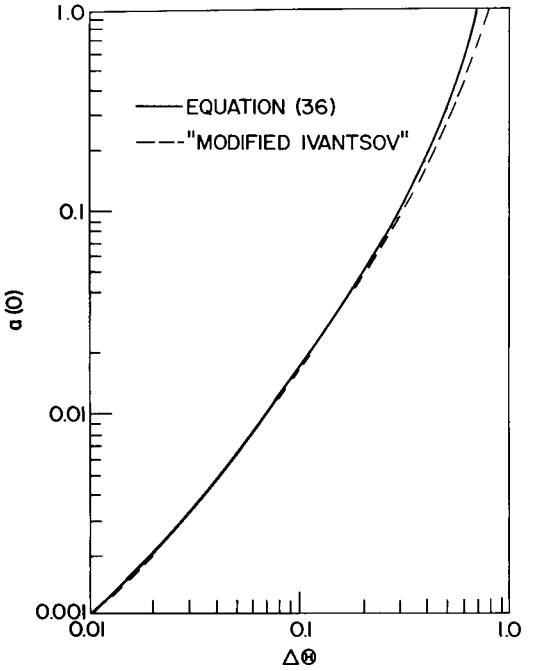

Fig. 6—Tip radius $a(0)$ as a function of $\Delta\Theta$

COMPARISON WITH EXPERIMENTAL DATA

To compare theory and experiment, we assume that the steady-state solution for $\lambda = \lambda_{max}$ represents the true asymptotic solution to the time-dependent dendrite growth problem (as assumed in Part 1) and that the theory can be applied with negligible error to materials having unequal solid and liquid thermal properties, provided that the

*In principle a more accurate estimate of $a(0)$ could be obtained by solving Eq. (28) with λ slightly less than λ^{**}. The numerical difficulties involved in obtaining reliable numerical solutions to Eq. (28) for $\lambda \approx \lambda^{**}$ however preclude such an estimate.

properties of the liquid are used with the theory. The first assumption is equivalent to the "maximum velocity" hypothesis, which is employed in virtually every theoretical treatment of steady-state dendritic growth. The second assumption is reasonable because the temperature gradient in the solid is generally small compared with that in the liquid; that is, $\bar{g}_e = O(1)$ and $\bar{g}_i = O(\lambda)$. Therefore the thermal properties of the solid have little influence on the steady-state shapes and growth rates.

The theory has been compared to experimental dendritic growth data for ice, nickel, and cobalt. The thermodynamic and transport properties of these materials are given in Table 4.

Table 4
Thermodynamic and Transport Properties (T_m is the equilibrium melting temperature (°C), L is the latent heat of fusion (cal/g), c_ℓ, ρ_ℓ, k_ℓ, and α_ℓ are the specific heat (cal/g-°K), density (g/cm^3), thermal conductivity (cal/s-cm-°K) and thermal diffusivity (cm^2/s) of the liquid at the melting temperature, ΔS_f is the entropy of fusion (cal/cm^3-°K), and $\gamma_{s\ell}$ is the solid/liquid interfacial free energy (erg/cm^2).)

Material	T_m	L	c_ℓ	ρ_ℓ	k_ℓ	α_ℓ	ΔS_f	$\gamma_{s\ell}$
H_2O	0	79.7	1.00	1.00	0.00139*	0.00139	0.292	45†
Ni	1453	69.7‡	0.176‡	8.0§	0.098*#	0.070	0.360	255¶
Co	1492	63.9‡	0.19‡	8.0**	0.06*#	0.040	0.322	234¶

*From Ref. 15.
†From Ref. 16.
‡From Ref. 17.
§From Ref. 18.
#Estimated from high-temperature data on k_s (thermal conductivity of the solid) using the relation $k_\ell/k_s = 1/2$ at T_m.
¶From Ref. 19.
**Assumed to have the same density as Ni.

The dendritic growth rates obtained by Pruppacher [4] and Hallett [5] for ice are shown as a function of the nondimensional supercooling $\Delta\Theta$ in Fig. 7. Also shown are the theoretical growth rates V obtained from the relation

$$V = \frac{2\alpha_\ell \Delta S_f L \lambda^*}{c_\ell \gamma_{s\ell}} \cdot \tag{37}$$

The agreement between theory and experiment is satisfactory for $0.02 < \Delta\Theta < 0.03$, with the experimental data dropping below the theoretical predictions for $\Delta\Theta > 0.03$. The disparity at the higher supercoolings is probably due to the effects of sluggish interfacial molecular attachment, an effect not accounted for in the theory at present.

The dendritic growth rates obtained by Walker [6] and Colligan and Bayles [7] for nickel and those obtained by Walker [6] for cobalt are shown in Figs. 8 and 9 along with the theoretical growth rates calculated with Turnbull's [19] values of $\gamma_{s\ell}$ using

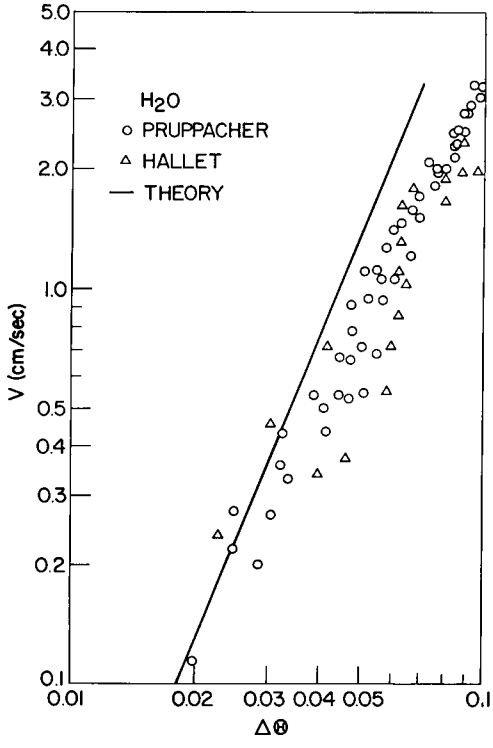

Fig. 7—Growth rate as a function of nondimensional supercooling for ice

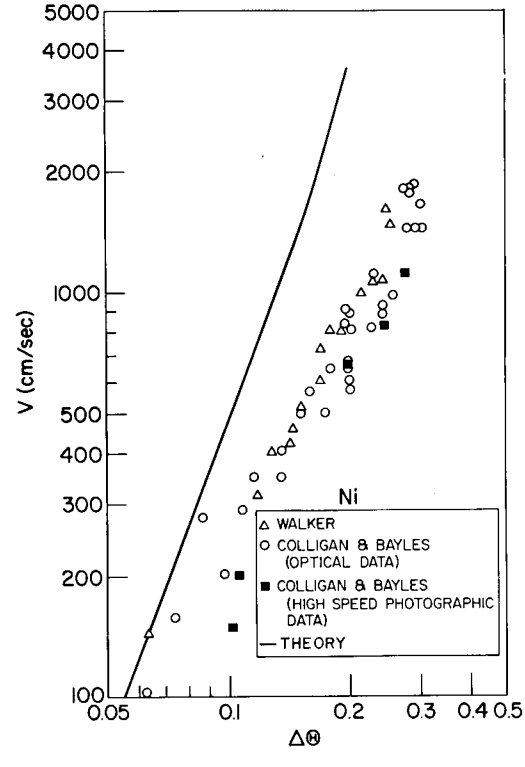

Fig. 8—Growth rate as a function of nondimensional supercooling for nickel

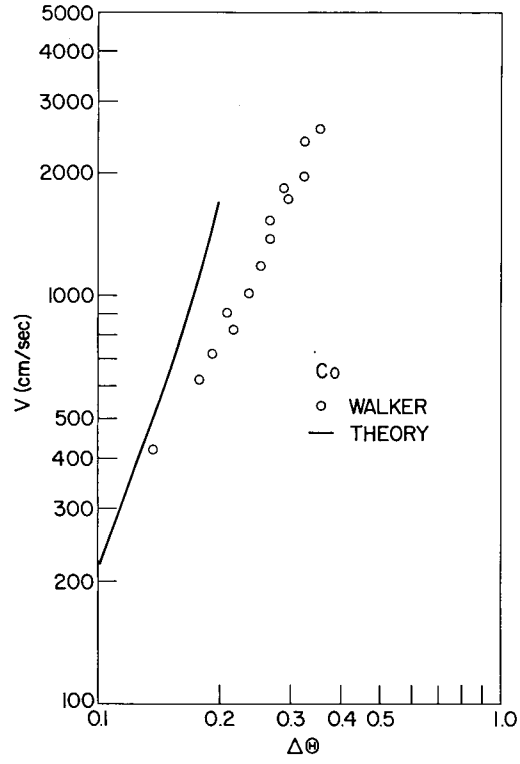

Fig. 9—Growth rate as a function of nondimensional supercooling for cobalt

Eq. (37). The theoretical growth rates are consistently higher than those observed experimentally for both materials, with the disparity increasing with increasing supercooling. Qualitatively it appears that the use of higher values of $\gamma_{s\ell}$ would improve the correlation between theory and experiment for both materials, particularly at the smaller supercoolings. This finding, though by no means conclusive, is consistent with recent measurements of $\gamma_{s\ell}$ for lead [20,21] and bismuth [22]; the reported values of $\gamma_{s\ell}$ were higher than Turnbull's values by factors of 2.2 and 1.5 respectively.

SUMMARY OF PART 2

Numerical results for the dendritic shape changes induced by nonisothermality were obtained as a function of the supercooling $\Delta\Theta$. The effect of the nonisothermal interface conditions is to increase the curvature of the interface in the neighborhood of the dendrite tip and to flatten it elsewhere.

Upper bounds λ^* on the maximum growth rate λ_{max} were computed for $0.01 \leqslant \Delta\Theta \leqslant 0.2$, and it was shown that λ^* provides a good approximation to λ_{max} over this range of supercoolings.

A second estimate λ^{**} to λ_{max} was computed over the aforementioned range of supercoolings. The two estimates λ^* and λ^{**} of λ_{max} are reasonably close (differing by a maximum of 15%), with the λ^* values providing the better estimate to λ_{max}.

The $\lambda^* - \Delta\Theta$ relation takes the form of a universal power law, namely, $\lambda^* = 0.057(\Delta\Theta)^{2.65}$, for $\Delta\Theta \leqslant 0.1$. Moreover the $\lambda^* - \Delta\Theta$ curve approaches the $\lambda_{max} - \Delta\Theta$ curve obtained from the "modified Ivantsov" analysis as the supercooling increases. The two curves essentially coalesce at $\Delta\Theta \approx 0.3 - 0.4$.

Estimates of the dendrite tip radii obtained with the present theory agree closely with those predicted by the "modified Ivantsov" analysis for $\Delta\Theta < 0.6$.

The λ^* $\Delta\Theta$ curve, when plotted on a logarithmic scale, is parallel to the $\lambda_{max} - \Delta\Theta$ curve obtained from Trivedi's analysis for $\Delta\Theta \leqslant 0.1$; however the growth rates predicted by the present theory are greater than those predicted by Trivedi's analysis by a factor of 2.3.

The dendritic growth rates predicted by the theory are in qualitative agreement with experimental data for ice, nickel, and cobalt.

Recommendations for future work include:

- further comparison of theory with experiment in the low supercooling range, particularly for materials for which $\gamma_{s\ell}$ is known independently,

- generalization of the theory to include the effects of interfacial "drag" from sluggish molecular attachment, and

- initiation of a time-dependent study of dendritic growth to verify the "maximum growth rate" hypothesis, determine the origin of dendritic side branching, and assess the influence of side-branch growth on the tip velocity.

REFERENCES

1. R.F. Sekerka, R.G. Seidensticker, D.R. Hamilton, and J.D. Harrison, "Investigation of Desalination by Freezing," Westinghouse Research Laboratories Report, 1967 Chapter 3.
2. M.E. Glicksman and R.J. Schaefer, *J. Crystal Growth* **1** (1967) 297.
3. R. Trivedi, private communication.
4. H.R. Pruppacher, *J. Colloid and Interface Sci.* **25** (1967) 285.
5. J. Hallett, *J. Atmos. Sci.* **21** (1964) 671.
6. J.L. Walker, unpublished work, presented in *Principles of Solidification*, B. Chalmers, New York, J. Wiley, 1964, Chapter 4.
7. G.A. Colligan and B.J. Bayles, *Acta Met.* **10** (1962) 895.
8. G.F. Bolling and W.A. Tiller, *J. Applied Phys.* **32** (1961) 2587.
9. D.E. Temkin, *Dokl. Akad. Nauk SSSR* **132** (1960) 1307.
10. P.J. Davis and P. Rabinowitz, *Numerical Integration*, Waltham, Mass., Blaisdell Pub. Co., 1967.

11. S.G. Mikhlin, *Variational Methods in Mathematical Physics*, New York, Pergamon, 1964, Chapter 9.

12. J.G.F. Francis, *Computer J.* 4 (1961) 265.

13. R. Trivedi, *Acta Met.* **18** (1970) 287.

14. M.E. Glicksman and R.J. Schaefer, *J. Crystal Growth* **2** (1968) 239.

15. Y.S. Touloukian, R.W. Powell, C.Y. Ho, and P.G. Klemens, *Thermophysical Properties of Materials*, Volume 1, New York, Plenum Press, 1970.

16. D.R.H. Jones, *Phil. Mag.* **27** (1973) 569.

17. J.L. Margrave, "Thermodynamic Properties of Liquid Metals," unpublished manuscript.

18. G.A. Colligan, W.T. Loomis, and V.A. Surprenant, *J. Australian Inst. of Metals* **10** (1965) 89.

19. D. Turnbull, *J. Applied Phys.* **21** (1950) 1022.

20. M.J. Stowell, *Phil. Mag.* **22** (1970) 1.

21. G.E. Nash and M.E. Glicksman, *Phil. Mag.* **24** (1971) 577.

22. M.E. Glicksman and C.L. Vold, *Scripta Met.* **5** (1971) 493.

23. L.M. Milne-Thomson, "Elliptic Integrals," p. 587 in *Handbook of Mathematical Functions*, M. Abramowitz and I.A. Stegun, editors, New York, Dover, 1965, and Washington, D.C.: U.S. Govt. Print. Off., 1964, ninth printing, Nov. 1970, with corrections.

Appendix A

THE BEHAVIOR OF $C_1(r,s)$ AND $C_2(r,s)$ AS $s \to r$ AND NUMERICAL COMPUTATION PROCEDURES

BEHAVIOR OF $C_2(r,s)$ AS $s \to r$

The behavior of $C_2(r,s)$ as $s \to r$ is readily ascertained by writing $C_2(r,s)$ as

$$C_2(r,s) = \frac{s}{\pi} e^{-[\omega_0(r)-\omega_0(s)]} G[r, \omega_0(r), s, \omega_0(s)]$$

$$= \frac{s}{\pi} e^{-[\omega_0(r)-\omega_0(s)]} \int_{-1}^{+1} e^{-(a+bt)^{1/2}} [(a+bt)(1-t^2)]^{-1/2} \, dt \tag{A1a}$$

$$= \frac{s}{\pi} e^{-[\omega_0(r)-\omega_0(s)]} (I_1 + I_2) , \tag{A1b}$$

where

$$a = s^2 + r^2 + [\omega_0(r) - \omega_0(s)]^2 , \tag{A2}$$

$$b = 2rs , \tag{A3}$$

$$\omega_0(r) = -r^2/2a_0 ,$$

$$\omega_0(s) = -s^2/2a_0 ,$$

$$I_1 = \int_{-1}^{+1} \frac{1}{(a+bt)^{1/2}(1-t^2)^{1/2}} \, dt ,$$

$$I_2 = \int_{-1}^{+1} \left[e^{-(a+bt)^{1/2}} - 1\right] [(a+bt)(1-t^2)]^{-1/2} \, dt ,$$

and examining the behavior of I_1 and I_2 as $a \to b$.

Expanding the exponential term in I_2 in a Taylor series, integrating term by term, and employing the transformation $t = \cos \xi$ gives

$$I_2 = \sum_{k=1}^{\infty} \frac{1}{(2k)!} \int_0^{\pi} (a + b\cos\xi)^{(2k-1)/2}\, d\xi - \sum_{k=0}^{\infty} \frac{1}{(2k+1)!} \int_0^{\pi} (a + b\cos\xi)^{k}\, d\xi ,$$

which is evidently bounded as $a \to b$. On the other hand the integral I_1 can be written as

$$I_1 = \int_{-1}^{+1} \frac{1}{(a+bt)^{1/2}(1-t^2)^{1/2}}\, dt$$

$$= \int_0^{\pi} (a + b\cos\xi)^{-1/2}\, d\xi$$

$$= \frac{2}{(a+b)^{1/2}} K\left(\left(\frac{2b}{a+b}\right)^{1/2}\right),$$

where $K(x)$ denotes the complete elliptic integral of the first kind. However, $K(x)$ has the known limiting behavior [23]

$$\lim_{x\to 1}\left[K(x) + \ln\left(\frac{\sqrt{1-x^2}}{4}\right)\right] = 0 . \tag{A4}$$

Therefore, as $s \to r$,

$$I_1 \approx -\frac{1}{r}\ln\left(\left\{\frac{(r-s)^2 + [\omega_0(r) - \omega_0(s)]^2}{64r^2}\right\}^{1/2}\right)$$

$$= -\frac{1}{r}\ln\left\{\frac{|r-s|[1+\omega_0'(r)]^{1/2}}{8r}\right\} = -\frac{1}{r}\ln\left[\frac{|r-s|}{8r\cos\theta_0(r)}\right].$$

Hence $C_2(r,s)$ has a logarithmic singularity as $s \to r$.

COMPUTATION OF $C_2(r,s)$

Defining $\beta \equiv (a-b)^{1/2}$, it proves convenient to consider separately the three regions

$0 < \beta \leqslant \beta_1$ (region I) ,

$\beta_1 < \beta \leqslant \beta_2$ (region II) ,

$\beta_2 > \beta < \infty$ (region III) .

In regions II and III the integral in Eq. (A1a) can be accurately evaluated by Gauss-Chebyshev quadrature:

$$\int_{-1}^{+1} \frac{f(x)}{(1-x^2)^{1/2}}\, dx = \frac{\pi}{N} \sum_{i=1}^{N} f(x_i)\,, \quad x_i = \cos \frac{(2i-1)\pi}{2N}\,,$$

where N takes the values N_2 and N_3 in regions II and III respectively. In region I additional accuracy is requaired due to the close proximity of the singular point. Hence in this region Eq. (A1b) is used with I_1 evaluated using standard polynomial approximations to $K(x)$ [23] and I_2 evaluated by Gauss-Chebyshev quadrature with $N = N_1$. The values of β_1, β_2, N_1, N_2, and N_3 used in the computations are listed as a function of $\Delta\Theta$ in Table A1.

Table A1
Values Used in Computing $C_2(r,s)$

$\Delta\Theta$	β_1	β_2	N_1	N_2	N_3
0.0-0.01	0.1	1.0	10	10	5
0.02-0.1	0.5	1.0	10	10	5
0.2-0.3	1.0	5.0	20	20	10
0.4-0.5	1.0	5.0	20	20	10

BEHAVIOR OF $C_1(r,s)$ AS $s \to r$

The behavior of $C_1(r,s)$ as $s \to r$ may be assessed by rewriting Eq. (2), namely,

$$C_1(r,s) = \frac{s}{\pi}\, e^{-[\omega_0(r)-\omega_0(s)]} \int_{-1}^{+1} e^{-(a+bt)^{1/2}} \left\{ \frac{\sin\theta_0(s)}{2s(a+bt)^{1/2}} - \left[\frac{1}{a+bt} + \frac{1}{(a+bt)^{3/2}} \right] \left\{ (s+rt)\sin\theta_0(s) - [\omega_0(s) - \omega_0(s)]\cos\theta_0(s) \right\} \right\} \frac{1}{(1-t^2)^{1/2}}\, dt, \tag{A5}$$

as

$$C_1(r,s) = \frac{s}{\pi}\, e^{-[\omega_0(r)-\omega_0(s)]} \left\{ A(r,s) \int_{-1}^{+1} e^{-(a+bt)^{1/2}} \left[(a+bt)^{-1} + (a+bt)^{-3/2} \right] (1-t^2)^{-1/2}\, dt - B(r,s) \int_{-1}^{+1} e^{-(a+bt)^{1/2}} (1-t^2)^{-1/2}\, dt \right\}$$

or

$$C_1(r,s) = \frac{s}{\pi} e^{-[\omega_0(r)-\omega_0(s)]} (I_3 + I_4 + I_5 + I_6) \tag{A6}$$

and examining the behavior of $A(r,s)$ and $I_k (k = 3, \ldots, 6)$ as $a \to b$. Here

$$I_3 = A(r,s) \int_{-1}^{+1} \left\{ e^{-(a+bt)^{1/2}} \left[(a+bt)^{-1} + (a+bt)^{-3/2}\right] - (a+bt)^{-3/2} \right.$$

$$\left. + \frac{1}{2} (a+bt)^{-1/2} \right\} (1-t^2)^{-1/2}\, dt\,, \tag{A7}$$

$$I_4 = -B(r,s) \int_{-1}^{+1} e^{-(a+bt)^{1/2}} (1-t^2)^{-1/2}\, dt\,,$$

$$I_5 = A(r,s) \int_{-1}^{+1} (a+bt)^{-3/2} (1-t^2)^{-1/2}\, dt\,,$$

$$I_6 = \frac{-A(r,s)}{2} \int_{-1}^{+1} (a+bt)^{-1/2} (1-t^2)^{-1/2}\, dt\,,$$

$$A(r,s) = \frac{\left\{r^2 - s^2 + [\omega_0(r) - \omega_0(s)]^2\right\} \sin\theta_0(s) + 2s[\omega_0(r) - \omega_0(s)] \cos\theta_0(s)}{2s}\,, \tag{A8}$$

$$B(r,s) = \frac{\sin\theta_0(s)}{2s}\,,$$

$$\sin\theta_0(s) = \frac{-\omega_0'(s)}{\left[1 + \omega_0'^2(s)\right]^{1/2}}\,,$$

$$\cos\theta_0(s) = \frac{1}{\left[1 + \omega_0'^2(s)\right]^{1/2}}\,.$$

It is evident from Eq. (A8) that $A(r,s) \to 0$ as $r \to s$. However, as will be apparent shortly, a more detailed knowledge of the asymptotic behavior of $A(r,s)$ is required. Hence expanding $A(r,s)$ in a Taylor series about $s = r$ gives

$$A(r,s) = \left(2s(r-s)\sin\theta_0(r) - 2s(r-s)^2 \frac{d}{dr} \sin\theta_0(r) + \left\{(r-s)^2 + [\omega_0(r)\right.\right.$$

$$\left. -\omega_0(s)]^2\right\} \sin\theta_0(r) - 2s(r-s)\sin\theta_0(r) - s\omega_0''(r)\cos\theta_0(r)(r-s)^2$$

$$\left. -2s\omega_0'(r)(r-s)^2 \frac{d}{dr} \cos\theta_0(r)\right) (2s)^{-1} + O(r-s)^3\,,$$

which, with the aid of Eq. (A2), reduces to

$$A(r,s) \approx \frac{\sin^3 \theta_0(r)}{2s \cos^2 \theta_0(r)} (r-s)^2 \tag{A9}$$

for s sufficiently close to r.

The limiting behavior of $I_k (k = 3, \ldots, 6)$ is now readily ascertained using the methods employed in the first section of this appendix. Hence, by writing I_5 and I_6 as

$$I_5 = A(r,s) \int_{-1}^{+1} (a + bt)^{-3/2} (1 - t^2)^{-1/2} \, dt$$

$$= A(r,s) \int_0^{\pi} (a + b \cos \xi)^{-3/2} \, d\xi$$

$$= \frac{2A(r,s)}{(a+b)^{1/2} (a-b)} E\left[\left(\frac{2b}{a+b}\right)^{1/2}\right]$$

and

$$I_6 = \frac{-A(r,s)}{(a+b)^{1/2}} K\left[\left(\frac{2b}{a+b}\right)^{1/2}\right],$$

where $E(x)$ denotes the complete elliptic integral of the second kind, the limiting values of I_5 and I_6 may be obtained with the aid of Eqs. (A4), (A9), and the relation [23]

$$\lim_{x \to 1} E(x) = 1 .$$

Thus

$$\lim_{s \to r} I_5 = \frac{\sin^3 \theta_0(r)}{2r^2} \tag{A10}$$

and

$$\lim_{s \to r} I_6 = \lim_{s \to r} \left[\frac{\sin^3 \theta_0(r)}{4r^3 \cos^3 \theta_0(r)} (r-s)^2 \ln\left(\frac{|r-s|}{2r \cos \theta_0(r)}\right)\right] = 0 , \tag{A11}$$

where the relations

$$\lim_{s \to r} (a + b) = (2r)^2$$

and

$$a - b \approx (r-s)^2 \left[1 + \omega_0'^2(r)\right] = (r-s)^2/\cos^2 \theta_0(r)$$

as $s \to r$ were used. Moreover, by expanding the exponential term in Eq. (A7) in a Taylor series and integrating term by term, it is readily seen that I_3 is bounded as $a \to b$. Thus, in view of Eq. (A9),

$$\lim_{s \to r} I_3 = 0 . \tag{A12}$$

Finally I_4, which can be written as

$$I_4 = -B(r,s) \int_{-1}^{+1} e^{-(a+bt)^{1/2}} (1-t^2)^{-1/2} \, dt$$

$$= -B(r,s) \int_{0}^{\pi} e^{-(a+b\cos\xi)^{1/2}} \, d\xi ,$$

is bounded as $s \to r$, with its limiting value given by

$$\lim_{s \to r} I_4 = -\frac{\sin\theta_0(r)}{2r} \int_{-1}^{+1} e^{-\sqrt{2}r(1+t)^{1/2}} (1-t^2)^{-1/2} \, dt . \tag{A13}$$

From the preceding discussion $C_1(r,s)$ is bounded as $r \to s$. In fact an expression for $C_1(r,r)$ is readily obtained with the aid of Eqs. (A6), (A10), (A11), (A12), and (A13). Thus

$$C_1(r,r) = -\frac{\sin\theta_0}{2\pi} \int_{-1}^{+1} e^{-\sqrt{2}r(1+t)^{1/2}} (1-t^2)^{-1/2} \, dt + \frac{\sin^3\theta_0(r)}{2\pi r} . \tag{A14}$$

COMPUTATION OF $C_1(r,s)$

It is again useful to employ the same regions used for $C_2(r,s)$ (regions I, II, and III). In regions II and III Eq. (A5) is used to compute $C_1(r,s)$, with the integral evaluated by an M-point Gauss-Chebyshev quadrature, where M takes the values M_2 and M_3 in regions II and III respectively. In region I, $C_1(r,s)$ is computed by means of Eq. (A1b), with the integrals appearing in I_3 and I_4 evaluated by an M_1-point Gauss-Chebyshev quadrature and I_5 and I_6 evaluated using polynomial approximations to $K(x)$ and $E(x)$ [23]. Finally $C_1(r,r)$ is computed from Eq. (A14), with the integral evaluated by an M_4-point Gauss-Chebshev quadrature. The values of β_1, β_2, M_1, M_2, M_3, and M_4 used in the computations are listed in Table A2.

Table A2
Values Used in Computing $C_1(r, s)$

$\Delta\Theta$	β_1	β_2	M_1	M_2	M_3	M_4
0.0-0.1	0.1	1.0	10	10	5	5
0.02-0.1	0.5	1.0	10	10	5	30
0.2-0.3	1.0	5.0	20	20	10	60
0.4-0.5	1.0	5.0	30	30	10	100